Inorganic Chemistry

Article

pubs.acs.org/IC

Activation of Rhenium(I) Toward Substitution in *fac*-[Re(*N,O′*-Bid)$(CO)_3(HOCH_3)$] by Schiff-Base Bidentate Ligands (*N,O′*-Bid)

Alice Brink,[†,‡] Hendrik G. Visser,[†] and Andreas Roodt*[,†,§]

[†]Department of Chemistry, [‡]Advanced Biomolecular Research Cluster, and [§]Materials and Nanosciences Cluster, University of the Free State, P.O. Box 339, Bloemfontein 9300, South Africa

Supporting Information

ABSTRACT: A series of *fac*-[Re(*N,O′*-Bid)$(CO)_3$(L)] (*N,O′*-Bid = monoanionic bidentate Schiff-base ligands with *N,O* donor atoms; L = neutral monodentate ligand) has been synthesized, and the methanol substitution reactions have been investigated. The complexes were characterized by NMR, IR, and UV−vis spectroscopy. X-ray crystal structures of the compounds *fac*-[Re(Sal-*m*Tol)$(CO)_3(HOCH_3)$], *fac*-[Re(Sal-*p*Tol)$(CO)_3(HOCH_3)$], *fac*-[Re(Sal-Ph)$(CO)_3(HOCH_3)$], and *fac*-[Re(Sal-Ph)$(CO)_3$(Py)] (Sal-*m*Tol = 2-(*m*-tolyliminomethyl)phenolato; Sal-*p*Tol = 2-(*p*-tolyliminomethyl)phenolato; Sal-Ph = 2-(phenyliminomethyl)phenolato; Py = pyridine) are reported. Significant activation for the methanol substitution is induced by the use of the *N,O* bidentate ligand as manifested by the second order rate constants, with limiting kinetics being observed for the first time. Rate constants (25 °C) (k_1 or k_3) and activation parameters ($\Delta H_k^{\ddagger}$, kJ mol^{-1}; $\Delta S_k^{\ddagger}$, J K^{-1} mol^{-1}) from Eyring plots for entering nucleophiles as indicated are as follows: *fac*-[Re(Sal-*m*Tol)$(CO)_3(HOCH_3)$] 3-chloropyridine: (k_1) 2.33 ± 0.01 M^{-1} s^{-1}; 85.1 ± 0.6, 48 ± 2; *fac*-[Re(Sal-*m*Tol)$(CO)_3(HOCH_3)$] pyridine: (k_1) 1.29 ± 0.02 M^{-1} s^{-1}; 92 ± 2, 66 ± 7; *fac*-[Re(Sal-*m*Tol)$(CO)_3(HOCH_3)$] 4-picoline: (k_1) 1.27 ± 0.05 M^{-1} s^{-1}; 88 ± 2, 53 ± 6; (k_3) 3.9 ± 0.03 s^{-1}; 78 ± 8, 30 ± 27; (k_f) 1.7 ± 0.02 M^{-1} s^{-1}; 86 ± 2, 49 ± 6; *fac*-[Re(Sal-*m*Tol)$(CO)_3(HOCH_3)$] DMAP (k_3) 1.15 ± 0.02 s^{-1}; 88 ± 2, 52 ± 7. An interchange dissociative mechanism is proposed.

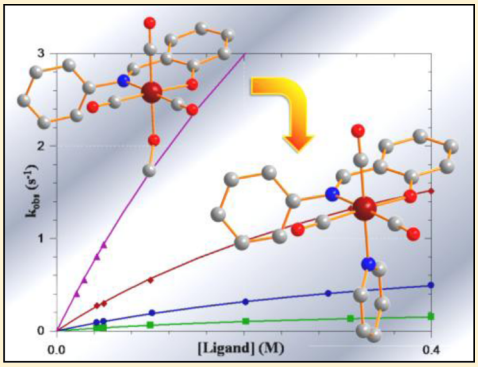

INTRODUCTION

The rich coordination chemistry of metal ions and the wide range of possible nuclear properties provide considerable interest for the development of radiopharmaceuticals. This is especially true for the Group 7 transition metals, in particular ^{99m}Tc, which is extensively utilized in diagnostic nuclear medicine.[1,2] Unsurprisingly, a significant interest in the organometallic technetium and rhenium tricarbonyl complexes in low oxidation states have occurred during the past 20 years for the development of target specific radiopharmaceuticals.[3−10] In particular the novel mild synthetic reaction conditions of stable organometallic Re(I) and Tc(I) moieties described by Alberto et al.[11] allow these moieties to be a serious contender in the design of target specific radiopharmaceuticals. The *fac*-$[M(CO)_3(H_2O)_3]^+$ complex (M = Re^I, Tc^I) is an attractive radiopharmaceutical synthon because of the high stability of the *fac*-$[M(CO)_3]^+$ core in water and the potential of exchanging the labile solvent ligands. An intriguing feature of the *fac*-$[M(CO)_3]^+$ core is its kinetic stability with various entering ligands. With the use of an appropriate ligand system, such as tridentate ligands or [2 + 1] ligand systems, the coordination sphere can be "closed", thus protecting the metal center from further interactions. As the *fac*-$[M(CO)_3(H_2O)_3]^+$ accepts many types of ligands, it is possible to design complexes whose properties such as hydro/lipophilicity are adapted to those of the biomolecule.

Rhenium with its $^{186/188}$Re β^--emitting isotopes has potential as a radiotherapeutic agent and is complementary to the diagnostic capability of ^{99m}Tc. Rhenium complexes have been investigated as models for Tc analogues because of related chemistries. To ensure the development of methods by which these radionuclides (^{99m}Tc, $^{186/188}$Re) can be included into appropriate radiopharmaceuticals, a knowledge of kinetics, reactivity, and mechanism of complex formation of the *fac*-$[M(CO)_3(H_2O)_3]^+$ with a diversity of chelating entering ligands with different binding atoms is important. From this focal point, their kinetic behavior is an aspect worth considering as it will influence the preparation, uptake, and clearance of the radiopharmaceutical agents.

A few valuable kinetic studies have been conducted on *fac*-$[M(CO)_3(H_2O)_3]^+$ complexes. The water exchange reaction[12] of *fac*-$[Re(CO)_3(H_2O)_3]^+$, a convenient measure for the intrinsic lability of the metal ion, was found to be $k_{ex} = 6.3(1) \times 10^{-3}$ s^{-1} and on the monohydroxo species $[Re^I(CO)_3(OH)(H_2O)_2]$, $k_{OH} = 27(1)$ s^{-1}. The basic form only contributed significantly to the kinetic exchange at $[H]^+ < 3 \times 10^{-3}$ M, and at higher $[H]^+$, the *fac*-$[Re(CO)_3(H_2O)_3]^+$ cation is the only exchanging species. Activation parameters for the water exchange process suggest a

Received: May 7, 2013
Published: July 24, 2013

   dx.doi.org/10.1021/ic401115j | *Inorg. Chem.* 2013, 52, 8950−8961

dissociative interchange mechanism (I_d) ($\Delta H^{\ddagger}$ = 90 ± 3 kJ mol^{-1}, $\Delta S^{\ddagger}$ = 14 ± 10 J K^{-1} mol^{-1}).

Studies on the water substitution reaction indicate that the three coordinated H_2O ligands of *fac*-$[Re(CO)_3(H_2O)_3]^+$ are readily substituted by monodentate ligands (trifluoroacetate, acetonitrile, thiourea, dimethylsulfide, and I^-) to form the mono-, bi-, and tri- coordinated complexes.[12−15] Substitution rates are found to be slightly dependent on the nature of the entering ligand, with the softer S-bonded ligands coordinating faster to the Re metal center than the O- and N-bonded ligands. Mechanistic changes occur from I_d for the harder ligands to I_a for softer ligands, such as dimethylsulfide and thiourea which are better nucleophiles.

Few substitution studies on complexes with the general form of *fac*-$[M(L,L'\text{-Bid})(CO)_3(H_2O)]^{n+}$ (*L*,*L*′-Bid = neutral or monoanionic bidentate ligands) are available. The potential use of bidentate ligands to activate the reasonably inert M(I)-tricarbonyl center, according to the [2 + 1] mixed ligand approach[16] could efficiently tailor these type of complexes for use in radiopharmacy. The use of bidentate ligands effectively blocks two of the reactive aqua sites, thus leaving one site open for substitution. A recent comprehensive study on the substitution of the third position can be found.[17,18] The bidentate ligands were selected to investigate complexes with a overall positive (*N*,*N*′-Bid ligand) to a neutral charge (*O*,*O*′-Bid and *N*,*O*-Bid ligand) with varied Brønsted basicities manifested by the corresponding pK_a values for the *L*,*L*′-BidH ligands. A four order-of-magnitude of activation for the methanol substitution was induced as indicated by the second order rate constants with (*N*,*N*′-Bid) < (*N*,*O*-Bid) < (*O*,*O*′-Bid). Significant activation of the rhenium(I) metal center was observed for *O*,*O*′-Bid type ligand systems.

Our interest is in the design of potential bifunctional chelator ligand systems for use in organometallic radiopharmacy. A primary focus is the introduction of the directing biomolecule onto a relatively small organic backbone before coordination to a radionuclide. With this as principal focus we have concentrated on the Schiff-base ligands as they represent a widely utilized and versatile ligand system, which can be easily manipulated, specifically electronically. Thus far, few salicylidene-type *fac*-$[M(CO)_3]^+$ complexes (M = Re^I, Tc^I) have been synthesized[19,20] and to the best of our knowledge, only one crystal structure of the *fac*-$[M(Sal)(CO)_3(H_2O)]$ (Sal = salicylidene or functionalized iminomethylphenolato ligands) has been published by groups other than ourselves.[21,22] Several aspects should be considered in the design of radiopharmaceuticals,[11] including the reactivity of the specific metal complexes with respect to different dynamic processes, as illustrated and discussed previously.[23−29] We thus report here the first kinetic study of Re(I) methanol substitution manipulated by the coordination of the salicylidene bidentate ligand system in *fac*-$[Re(Sal)(CO)_3(HOCH_3)]$ (Sal: Sal-*m*Tol = 2-(*m*-tolyliminomethyl)phenolato; Sal-Ph = 2-(phenyliminomethyl)phenolato; Sal-*p*Tol =2-(*p*-tolyliminomethyl)phenolato) with a range of entering monodentate ligands. A crystallographic study on the reactants as well as products, to fully characterize the starting complexes was initiated and four representative crystal structures, are reported here to illustrate the orientation of the coordinated methanol and monoligated complexes. The crystal structures are among the first published structures by our research group of *fac*-$[Re(CO)_3]^+$ containing a coordinated methanol solvent ligand in the sixth position.

EXPERIMENTAL SECTION

General Procedures. All experiments were performed aerobically using double distilled water and methanol. Unless otherwise stated, all chemicals were of reagent grade and purchased from Sigma Aldrich. Rhenium pentacarbonyl bromide was purchased from Strem Chemicals, Newburyport, U.S.A. *fac*-$[NEt_4]_2[ReBr_3(CO)_3]$ was synthesized as described by Alberto et al.,[30,31] while the ligands, 2-(*m*-tolyliminomethyl)phenol (SalH-*m*Tol) (**1**), 2-(*p*-tolyliminomethyl)-phenol (SalH-*p*Tol) (**2**), and 2-(phenyliminomethyl)phenol (SalH-Ph) (**3**) were synthesized according to literature procedures.[21,32,33] The ^{13}C and ^1H FT-NMR spectra were recorded at 150.96 and 600.28 MHz respectively on a Bruker AXS 600 MHz at 25 °C in CD_3OD (3.31 ppm), C_3H_6O (2.05 ppm) and $CDCl_3$ (7.26 ppm); chemical shifts are reported in parts per million (ppm). ^{13}C NMR spectra were calibrated relative to the ^{13}C resonances for CD_3OD (49.0 ppm), C_3H_6O (29.8 ppm), and $CDCl_3$ (77.2 ppm). The long relaxation times of specifically the carbonyl ligands, together with the low solubility of most of the complexes, result in many of these not being observed by ^{13}C NMR. The presence of the carbonyl ligands were however clearly detected by IR spectroscopy and X-ray diffraction. Infrared spectra were recorded on a Bruker Tensor 27 Standard System spectrophotometer with a laser range of 4000−370 cm^{-1}, equipped with a temperature cell regulator, accurate within 0.3 °C. Solid samples were analyzed as KBr pellets. All data were recorded at ambient temperature. UV−vis spectra were collected on a Varian Cary 50 Conc UV−visible Spectrophotometer, equipped with a Julabo F12-mV temperature cell regulator (accurate within 0.05 °C) in a 1.000 ± 0.001 cm quartz tandem cuvette. Rapid kinetic reactions ($t_{1/2}$< 20 s) were evaluated on a Hi-Tech SF-61DX2 Stopped-flow System attached to a Julabo F12-mV temperature regulator (accurate within 0.05 °C). The Stopped-flow System is capable of multiple wavelength detection in the diode-array mode (dead time <5 ms; 400 nm spectral width scans collected at <5 ms/complete scan), with a thermostatted SHU61DX sample handling unit, in which the initial reactions were collected to find the appropriate wavelength of the absorbance changes. After the specific wavelength was selected, the stopped-flow system was changed to the more sensitive photomultiplier mode (dead time ca. 1 ms) to study the rapid kinetic reactions. The values reported (see Supporting Information) consist of the average of four individual traces per concentration.

***fac*-[Re(Sal-*m*Tol)(CO)$_3$(HOCH$_3$)] (4).** $[NEt_4]_2[ReBr_3(CO)_3]$ (300 mg, 0.39 mmol) was dissolved in methanol (15 mL). $AgNO_3$ (198 mg, 1.2 mmol) was added, and the reaction stirred for 26 h at room temperature and then the AgBr precipitated and was filtered. SalH-*m*Tol (86.4 mg, 0.41 mmol) dissolved in methanol (10 mL) was added dropwise, where after the reaction mixture was heated to 70 °C and stirred for 14 h. The majority of the solvent was removed under reduced pressure before allowing the yellow solution to evaporate slowly. Crystals suitable for X-ray diffraction were obtained. (Yield of crystalline product: 81.7 mg, 41%). IR (KBr, cm^{-1}): $\nu_{(CO)}$= 2002 (s), 1869 (s). UV−vis (nm, M^{-1} cm^{-1}): λ_{max} = 398, ε = 3139. Anal. Calcd.: C, 42.18; H, 3.15; N, 2.73. Anal. Found: C, 42.43; H, 3.27; N, 2.69. ^1H NMR (600 MHz, acetone-d_6) δ2.40 (s, 3H), 2.96 (bs, 3H), 7.28 (m, 3H), 7.37 (m, 5H), 8.21 (s, 1H). $^{13}C\{^1H\}$ NMR (600 MHz, acetone-d_6) δ21.4, 114.3, 121.1, 121.3, 123.3, 124.5, 127.4, 129.1, 135.3, 137.0, 137.1, 158.7, 167.7, 166.6.

***fac*-[Re(Sal-*m*Tol)(CO)$_3$(Py)] (5).** $AgNO_3$ (66.1 mg, 0.39 mmol) was added to $[NEt_4]_2[ReBr_3(CO)_3]$ (100 mg, 0.13 mmol) dissolved in methanol. The reaction was stirred for 26 h at room temperature followed by the filtering of the precipitated AgBr. SalH-*m*Tol (28.8 mg, 0.16 mmol) was added, and the reaction stirred at 74 °C for 14 h. Pyridine (Py) (10.3 mg, 0.13 mmol) was then added to the warm solution and again stirred for 1 h. The excess solvent was removed, and the product crystallized at 4 °C. (Yield crystalline product: 49.2 mg, 68%). IR (KBr, cm^{-1}): $\nu_{(CO)}$ = 2015 (m), 1891 (s). UV−vis (nm, M^{-1} cm^{-1}): λ_{max} = 402, ε = 2345. Anal. Calcd.: C, 47.22; H, 3.06; N, 5.01. Anal. Found: C, 47.08; H, 3.04; N, 5.09. ^1H NMR (600 MHz, acetone-d_6) δ2.34 (s, 3H), 6.58 (m, 1H), 6.84 (m, 1H), 6.86 (s, 1H), 6.90 (m, 1H), 7.12 (m, 1H), 7.31 (m, 2H), 7.38 (m, 1H), 7.59 (m, 1H), 8.08 (m, 1H), 8.30 (s, 1H), 8.61 (m, 2H). $^{13}C\{^1H\}$ NMR (600 MHz, acetone-d_6)

dx.doi.org/10.1021/ic401115j | Inorg. Chem. 2013, 52, 8950−8961

δ 21.4, 115.9,121.2, 121.5, 123.4, 124.6, 126.9, 128.1, 129.7, 136.4, 137.2, 139.8, 140.4, 152.9, 157.4, 166.9, 168.0.

***fac*-[Re(Sal-*p*Tol)(CO)$_3$(HOCH$_3$)] (6).** The complex, *fac*-[Re(Sal-*p*Tol)(CO)$_3$(HOCH$_3$)], was synthesized in a similar way as (**4**) using $AgNO_3$ (198 mg, 1.2 mmol), $[NEt_4]_2[ReBr_3(CO)_3]$ (300 mg, 0.39 mmol) and SalH-*p*Tol (86.4 mg, 0.41 mmol). The product crystallized at 4 °C. (Yield crystalline product: 174.0 mg, 87%). IR (KBr, cm^{-1}): $\nu_{(CO)}$ = 2020 (m), 1892 (s). UV−vis (nm, M^{-1} cm^{-1}): λ_{max} = 386, ε = 2032. Anal. Calcd.: C, 42.18; H, 3.15; N, 2.73. Anal. Found: C, 42.35; H, 3.31; N, 2.88. ^{1}H NMR (600 MHz, acetone-d_6) δ2.39 (s, 3H), 6.57 (m, 1H), 6.80 (m, 1H), 7.19 (m, 2H), 7.26 (bs, 2H), 7.35 (m, 2H), 8.36 (s, 1H). ^{13}C{^{1}H} NMR (600 MHz, acetone-d_6) δ 20.0, 114.5, 114.7, 122.0, 122.2, 122.8, 122.9, 129.2, 129.3, 135.0, 135.3, 136.2, 155.2, 166.9.

***fac*-[Re(Sal-Ph)(CO)$_3$(HOCH$_3$)] (7).** The ligand SalH-Ph (14.6 mg, 0.074 mmol) dissolved in methanol (5 mL) was added to $[NEt_4]_2[ReBr_3(CO)_3]$ (41.0 mg, 0.053 mmol) in methanol (5 mL). The reaction was heated to 75 °C for 12 h. The yellow solution was allowed to evaporate slowly, and crystals suitable for X-ray diffraction were grown from methanol at 5 °C. (Yield crystalline product: 15.4 mg, 58%). IR (KBr, cm^{-1}): $\nu_{(CO)}$= 2021 (m), 1893 (s). UV−vis (nm, M^{-1} cm^{-1}): λ_{max} = 402, ε = 3717. Anal. Calcd.: C, 40.96; H, 2.83; N, 2.81. Anal. Found: C, 41.03; H, 2.77; N, 2.85. ^{1}H NMR (600 MHz, acetone-d_6) δ6.50 (m, 1H), 6.75 (d, 1H, J = 8.5 Hz), 7.25 (m, 5H), 7.40 (m, 2H), 8.24 (s, 1H). ^{13}C{^{1}H} NMR (600 MHz, acetone-d_6) δ113.5, 120.4, 120.5, 122.5, 123.1, 125.8, 128.5, 128.7, 134.5, 136.1, 157.8, 165.8, 166.6.

***fac*-[Re(Sal-Ph)(CO)$_3$(Py)] (8).** The ligand SalH-Ph (28.0 mg, 0.14 mmol) dissolved in methanol (5 mL) was added to a methanol (10 mL) solution of $[NEt_4]_2[ReBr_3(CO)_3]$ (100 mg, 0.13 mmol). The reaction was stirred for 4 h at 25 °C before the addition of pyridine (15.0 mg, 0.19 mmol) followed by a further 12 h stirring. The yellow precipitate was filtered and dried. Crystals suitable for X-ray diffraction were obtained from the slow evaporation of the filtrate. (Yield: 45.8 mg, 65%). IR (KBr, cm^{-1}): $\nu_{(CO)}$ = 2015 (s), 1907 (s), 1885 (s). UV−vis (nm, M^{-1} cm^{-1}): λ_{max} = 407, ε = 2487. Anal. Calcd.: C, 46.23; H, 2.77; N, 5.14. Anal. Found: C, 46.00; H, 2.59; N, 5.12. ^{1}H NMR (600 MHz, acetone-d_6) δ6.58 (m, 1H), 6.90 (d, 1H, J = 8.5 Hz), 7.06 (m, 2H), 7.31 (m, 2H), 7.38 (m, 1H), 7.47 (m, 2H), 7.58 (m, 3H), 8.07 (m, 1H), 8.32 (s, 1H), 8.62 (m, 2H). ^{13}C{^{1}H} NMR (600 MHz, acetone-d_6) δ 115.0, 120.6, 122.6, 123.1, 123.5, 126.1, 126.6, 128.1, 129.0, 135.6, 136.4, 139.2, 139.5, 152.0, 154.4, 156.6, 166.1, 167.4.

Table 1 gives a summary of the spectroscopic data for the different complexes.

X-ray Crystallography. Diffraction data for **4**, **6**, and **7** were collected on a Bruker X8 ApexII 4K diffractometer[34] using Mo *Kα* radiation with *ω*-and-*φ*-scans at 100 K. COSMO[35] was utilized for optimum collection of more than a hemisphere of reciprocal space. Frame integration and data reduction were performed using the Bruker SAINT-Plus and XPREP[36] software packages, respectively. Data was corrected for absorption effects using the multiscan technique SADABS.[37] The data for **8** was collected on an Oxford Diffraction Xcalibur 3 Crysalis CCD system[38] using Mo K*α* (0.71069 Å) and *ω*-scans. Intensity data were extracted and integrated using Crysalis RED.[39] The structures were solved by direct methods package SIR97[40] and refined using the software package WinGX,[41] incorporating SHELXL.[42] All non-hydrogen atoms were refined with anisotropic displacement parameters, while the methyl, methane, and aromatic H atoms were placed in geometrically idealized positions and constrained to ride on their parent atoms, with (C−H = 0.98−0.95 Å and U_{iso}(H) = 1.5U_{eq}(C) and 1.2U_{eq}(C)), respectively. The methyl protons were located from a difference Fourier map, and the group was refined as a rigid motor. A large electron density peak/hole is often found within about 1 Å from the Re^I metal centers for most structures and are attributed to the modeling of the absorption correction. The program DIAMOND[43] was used for all graphical representation of the crystal structures. All structures are shown with thermal ellipsoids drawn at 50% probability level unless otherwise stated. Graphical representations of overlays of selected complexes are obtained with Hyperchem 7.52.[44] The data collection and refinement data are given in Table 2, while selected interatomic bond distances and angles are reported in Table 3.

Table 1. Comparison of Spectroscopic Data for *fac*-[Re(*L*,*L*′-Bid)(CO)$_3$(L)] Complexes[a]

compound	λ_{max} (nm)	ε (M^{-1} cm^{-1})	$\nu_{(CO)}$ (KBr; cm^{-1})		
***N*,*O*-Bid**					
[Re(Sal-mTol)(CO)$_3$(HOCH$_3$)], **4**	398	3139	2002		1869
[Re(Sal-mTol)(CO)$_3$(Py)], **5**	402	2345	2015		1891
[Re(Sal-*p*Tol)(CO)$_3$(HOCH$_3$)], **6**	386	2032	2020		1892
[Re(Sal-Ph)(CO)$_3$(HOCH$_3$)], **7**	402	3717	2021		1893
[Re(Sal-Ph)(CO)$_3$(Py)], **8**	407	2487	2015	1907	1889
[Re(Sal-3MeBu)(CO)$_3$(HOCH$_3$)][b]	383	1311	2001		1877
[Re(Sal-3MeBu(CO)$_3$(Py)][b]	389	2038	2014	1905	1878
[Re(Pico) (CO)$_3$(H$_2$O)][c]	313	5140	2022	1908	1874
[Re(2,4-dPicoH)(CO)$_3$(H$_2$O)][c]	339	4280	2035	1919	--
[Re(2,4-dPicoH)(CO)$_3$(Py)][c]	315	5550	2030	1929	1908
[Re(2,4-dQuinH)(CO)$_3$(H$_2$O)][c]	352	51900	2034	1936	1886
[Re(2,4-dQuinH)(CO)$_3$(Py)][c]	358	49900	2024	1926	1869
***O*,*O*′-Bid**					
[Re(Flav)(CO)$_3$(H$_2$O)][c]	343	26500	2013	1885	
[Re(Flav)(CO)$_3$(Br)]$^-$[c]	342	25000	1999	1863	
[Re(Flav)(CO)$_3$(HOCH$_3$)][c]	343	26600	2015	1892	
[Re(Flav)(CO)$_3$(Py)][c]	342	25480	2012	1897	1860
[Re(Flav)(CO)$_3$(DMAP)][c]	344	15450	2006	1908	1888

[a]L = monodentate ligands as indicated. [b]Ref 21. [c]Ref 17.

Equilibrium Studies. The substitution of methanol in the *fac*-[Re(*L*,*L*′-Bid)(CO)$_3$(HOCH$_3$)] complexes for a range of entering ligands could be studied as pseudo first-order processes defined by the overall equilibrium as indicated in eq 1.

$$[Re(L, L'\text{-Bid})(CO)_3(HOCH)_3] + L \underset{k_{-1}}{\overset{k_1,K_1}{\rightleftharpoons}} [Re(L, L'\text{-Bid})(CO_3)(L)] + HOCH_3 \quad (1)$$

The overall stability constant (denoted by K_1) for the reaction between the *fac*-[Re(*L*,*L*′-Bid)(CO)$_3$(HOCH$_3$)] complex and the monodentate entering ligands (L) has been determined kinetically using the definition $K_1 = k_1/k_{-1}$. It was alternatively obtained by the nonlinear least-squares analysis using the established relationship based on UV−vis data, $A_{obs} = (A_M + A_{ML}K_1[L])/(1 + K_1[L])$, as reported previously[45] derived from Beer's law, mass balance, and the definition of K_1 for the overall reaction, where A_M and A_{ML} represent the absorbance of the *fac*-[Re(*L*,*L*′-Bid)(CO)$_3$(HOCH$_3$)] and *fac*-[Re(*L*,*L*′-Bid)-(CO)$_3$(L)] complexes, A_{obs} the observed absorbance, and [L] the concentration of the entering ligand, respectively, see Figure 1.[46]

Kinetic Studies. Stability tests were conducted over several days on a UV−vis spectrometer on the *fac*-[Re(*L*,*L*′-Bid)(CO)$_3$(HOCH$_3$)] complexes to ensure no ligand dissociation, decomposition, or dimerization occurred. Because of the poor solubility of some complexes in water and to ensure that the methanol solvated complexes remained intact, all reactions were performed in methanol. The use of dry freshly distilled methanol as solvent is essential, as a slow water exchange reaction is observed in reagent grade methanol. The methanol−water exchange reaction was not investigated further but is the subject of future studies.

dx.doi.org/10.1021/ic401115j | Inorg. Chem. 2013, 52, 8950−8961

Table 2. Summary of Crystal Data and Structure Refinement for *fac*-[Re(Sal-*m*Tol)(CO)$_3$(HOCH$_3$)] (4), *fac*-[Re(Sal-*p*Tol)(CO)$_3$(HOCH$_3$)] (6), *fac*-[Re(Sal-Ph)(CO)$_3$(HOCH$_3$)] (7), *fac*-[Re(Sal-Ph)(CO)$_3$(Py)] (8)

	4	6	7	8
empirical formula	$C_{18}H_{16}NO_5Re$	$C_{18}H_{16}NO_5Re$	$C_{17}H_{14}NO_5Re$	$C_{21}H_{15}N_2O_4Re$
FW	512.53	512.52	498.49	545.55
crystal system	monoclinic	monoclinic	monoclinic	monoclinic
space group	*C*2/*c*	*C*2/*c*	*C*2/*c*	$P2_1/c$
a (Å)	18.513(6)	19.370(4)	18.4769(7)	10.2910(2)
b (Å)	13.598(6)	14.027(3)	13.4830(7)	9.8280(2)
c (Å)	14.294(5)	14.002(3)	13.9281(7)	18.9306(3)
α (deg)	90	90	90	90
β (deg)	106.443(2)	112.41(3)	108.988(3)	97.023(2)
γ (deg)	90	90	90	90
V (Å^3)	3451(2)	3517(1)	3281.0(3)	1900.27(6)
Z	8	8	8	4
D_{calcd} (Mg m^{-3})	1.973	1.936	2.018	1.907
μ (mm^{-1})	7.070	6.938	7.433	6.424
T (K)	100	100	100	100
λ (Å)	0.71073	0.71073	0.71073	0.71069
crystal size (mm)	0.24 × 0.07 × 0.06	0.16 × 0.15 × 0.14	0.38 × 0.09 × 0.07	0.20 × 0.10 × 0.05
F(000)	1968	1968	1904	1048
R_{int}	0. 0611	0. 0958	0. 0805	0. 0309
GoF	1.073	1.210	1.084	1.022
R_1 [$I > 2\sigma(I)$]	R_1 = 0.0356, wR_2 = 0.0610	R_1 = 0.1073, wR_2 = 0.2046	R_1 = 0.0427, wR_2 = 0.0954	R_1 = 0.0352, wR_2 = 0.0887
R_1(all data)	R_1 = 0.0536, wR_2 = 0.0671	R_1 = 0.1657, wR_2 = 0.2575	R_1 = 0.0547, wR_2 = 0.1019	R_1 = 0.0442, wR_2 = 0.0925

Table 3. Selected Bond Distances (Å) and Angles (deg) for 4, 6, 7, and 8 (L = HOCH$_3$, Py)

	4	6		7	8
		Bond Distance			
Re1−N1	2.157(4)	2.15(2)		2.164(6)	2.152(5)
Re1−O1	2.119(3)	2.133(16)		2.121(5)	2.114(3)
Re1−C01	1.913(6)	1.90(3)		1.920(7)	1.925(5)
Re1−C02	1.919(6)	1.95(2)		1.909(7)	1.910(5)
Re1−C03	1.890(6)	1.89(2)		1.895(7)	1.904(6)
Re1−L	2.179(3)	2.24(10)[a]	2.17(3)[b]	2.188(5)	2.207(5)
N1−C1	1.290(6)	1.28(3)		1.288(9)	1.298(7)
		Bond Angle			
N1−Re1−O1	84.6(1)	84.8(7)		84.4(2)	84.54(16)
L−Re1−C03	175.4(2)	176(3)		174.9(3)	178.44(19)
Re1−O04−C04	122.1(4)	119(8)[a]	123.6(19)[b]	121.2(5)	
Re1−C02−O02	179.4(5)	176(3)		178.4(6)	178.9(5)
C1−N1−C21	115.7(4)	112(2)[a]		115.6(6)	114.4(5)
C26−C21−N1−C1	90.9(6)			100.6(8)	78.2(7)

[a/b] = disordered atoms.

Only one reaction was observed spectroscopically, under dry conditions, during this study for all the different entering ligands L investigated, see Figure 2.

All the kinetic runs were performed under *pseudo* first-order conditions with the ligand in large excess. Least-squares analyses were performed on the absorbance vs time data obtained from the kinetic runs to appropriate functions using MicroMath Scientist.[47] The solid lines in the figures represent computer least-squares fits of data, while experimental values are represented as individual points, denoted by selected symbols (Figure 2). The concentration dependence of the *pseudo* first-order rate constant (k_{obs}) for the substitution process of the methanol ligand in the *fac*-[Re(*L*,*L*′-Bid)(CO)$_3$(HOCH$_3$)] complexes by monodentate entering ligands (indicated by L) is given by eq 2[40,41] assuming the equilibrium process defined in eq 1 and monitoring of the kinetics at conditions where [L] ≫ [Re], with typical metal concentrations ranging from 1 × 10^{-4} to 5 × 10^{-4} M, see Figure 3a.

$$k_{obs} = k_1[L] + k_{-1} \quad (2)$$

However, the existence of a more complicated two-step interchange type mechanism, *I*, whereby there is an interchange with L in the outer-sphere complex ([Re(*L*,*L*′-Bid)(CO)$_3$(HOCH$_3$)]·····L) to form a rapid pre-equilibrium as described below, followed by a slower rate-determining second reaction as indicated in eq 3, is clearly also possible based on the k_{obs} vs [L] profiles, see Figure 3b and 3c.

$$[\mathrm{Re}(L, L'\text{-Bid})(\mathrm{CO})_3(\mathrm{HOCH})_3] + \mathrm{L} \overset{K_2}{\rightleftharpoons} [\mathrm{Re}(L, L'\text{-Bid})(\mathrm{CO}_3)(\mathrm{HOCH}_3)]\cdots(\mathrm{L})]$$

$$[\mathrm{Re}(L, L'\text{-Bid})(\mathrm{CO})_3(\mathrm{HOCH})_3]\cdots(\mathrm{L})] \underset{k_{-3}}{\overset{k_3}{\rightleftharpoons}} [\mathrm{Re}(L, L'\text{-Bid})(\mathrm{CO}_3)(\mathrm{L})] + \mathrm{HOCH}_3 \quad (3)$$

dx.doi.org/10.1021/ic401115j | Inorg. Chem. 2013, 52, 8950−8961

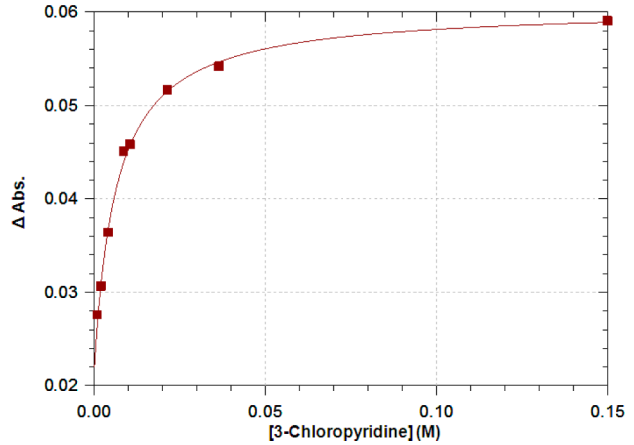

Figure 1. Plot of ΔAbs vs [Ligand] for the reaction between *fac*-[Re(Sal-*m*Tol)(CO)$_3$(HOCH$_3$)] and 3-chloropyridine at 25 °C in methanol, [Re complex] = 4.33 × 10^{-4} M, (λ = 436 nm), [3-ClPy] = 0.001 M–0.15 M.

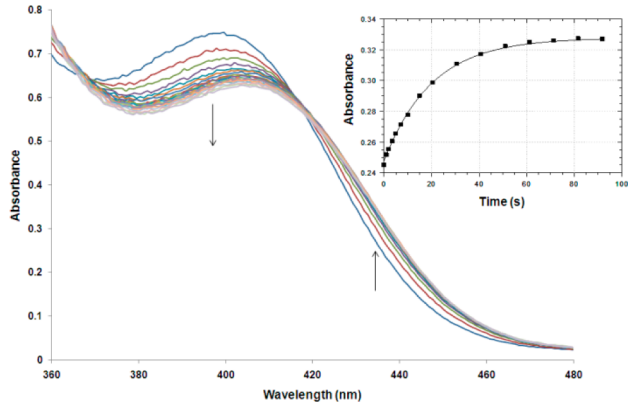

Figure 2. Typical UV–vis spectral change for the methanol substitution reaction of *fac*-[Re(Sal-*m*Tol)(CO)$_3$(HOCH$_3$)] with 3-chloropyridine in methanol at 15 °C, [Re complex] = 4.38 × 10^{-4} M, [3-ClPy] = 0.04 M, Δt = 1 s, t_{total} = 90 s. Inset represents the fit of Absorbance vs time data at 435 nm to a single exponential.[17]

The extent of the influence of the entering ligand (L) could affect whether the correct mechanism is I_d, I or I_a. The rate expression for this scheme, where [L] ≫ [M], is defined as indicated in eq 4.

$$k_{obs} = k_3K_2[L]/(1 + K_2[L]) + k_{-3} \quad (4)$$

In eq 4, K_2 is the pre-equilibrium constant, k_3 is the observed second-order limiting rate constant, and k_{-3} is the solvolysis rate constant indicated by the least-squares fits of k_{obs} vs [L].[48,49] The magnitude of K_2 will clearly be dependent on the strength of the interaction between the complex and the entering ligand L. The rate constants are reported in Table 4.

Activation parameters for the reactions with all the different entering ligands were determined from the corresponding Eyring plots,[49,50] see Figure 4, and the data thus obtained are reported in Table 4. The data for the 3-ClPy and pyridine were also globally fitted, and the values for the activation parameters obtained were in excellent agreement with those obtained from Figure 4, see Table 4.

Computational Experiments. Computational results were obtained using the GAUSSIAN-03W[51] software package. Density functional theory (DFT) calculations were performed at the B3LYP[52] level of theory with the 6-31G++(d,p)[53,54] basis set for the main group elements and LanL2Dz for rhenium, using the High Performance Computing Facility of the University of the Free State. Optimized structures were verified as minima through frequency analysis. The crystal structures are denoted with numerical values, for example SalH-

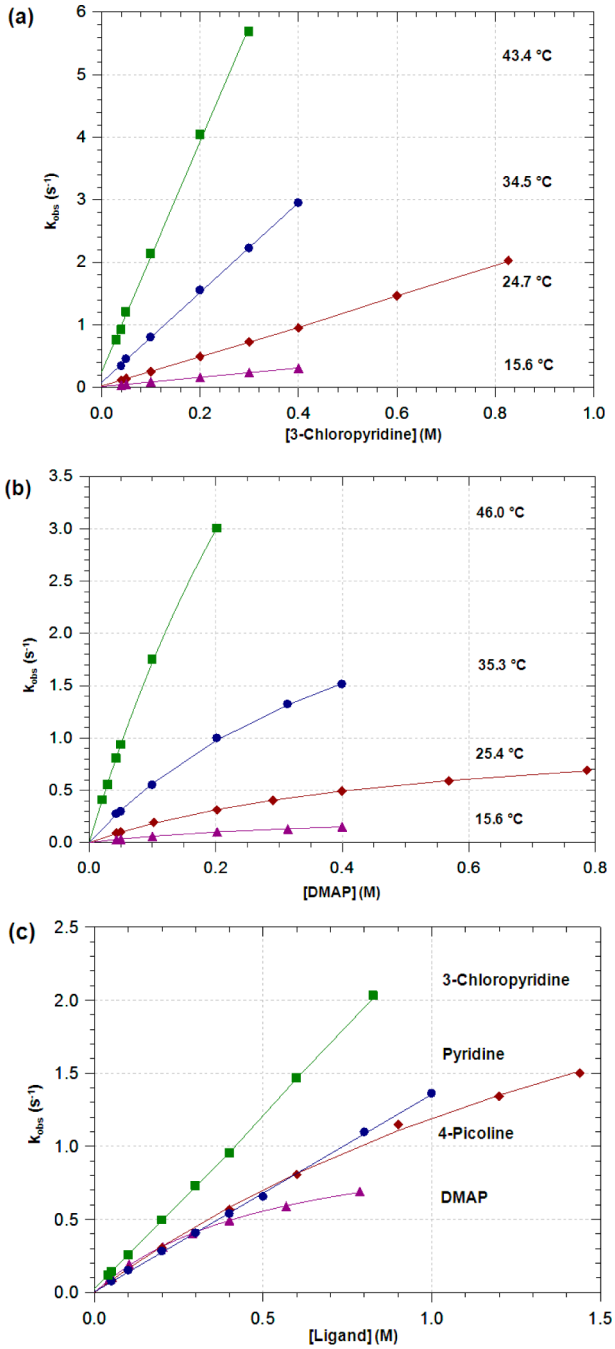

Figure 3. Plot of k_{obs} vs entering ligand for the reaction of (a) *fac*-[Re(Sal-*m*Tol)(CO)$_3$(HOCH$_3$)] and 3-chloropyridine at various temperatures in methanol, yielding linear plots, [Re complex] = 4.38 × 10^{-4} M, (λ = 436 nm); (b) *fac*-[Re(Sal-*m*Tol)(CO)$_3$(HOCH$_3$)] and DMAP at various temperatures in methanol yield limiting plots, [Re complex] = 5.19 × 10^{-4} M, (λ = 440 nm); (c) *fac*-[Re(Sal-*m*Tol)(CO)$_3$(HOCH$_3$)] and various entering ligands at 25 °C in methanol.

*m*Tol, *fac*-[Re(Sal-*m*Tol)(CO)$_3$(HOCH$_3$)], or *fac*-[Re(Sal-*m*Tol)-(CO)$_3$(Py)] are indicated as **1**, **4**, or **5**. The corresponding optimized structures are indicated as **1***, **4***, or **5***, respectively.

RESULTS AND DISCUSSION

Synthesis. Our interest is in the coordination of the Schiff-base type ligand to Re/Tc(I) tricarbonyl metal center, whereby a biologically active amine may be introduced onto the relatively

dx.doi.org/10.1021/ic401115j | Inorg. Chem. 2013, 52, 8950–8961

Table 4. Rate Constants at 25 °C and Activation Parameters for the Reaction of *N,O*-bidentate Ligand Complexes *fac*-[Re(Sal-*m*Tol)(CO)$_3$(HOCH$_3$)] with Different Entering Ligands in Methanol

ligand[a]		k_1	k_{-1}	K_1[b]	k_3	K_2[c]	k_f[d]	$\Delta H^{\ddagger}(k_1)$	$\Delta S^{\ddagger}(k_1)$
L	pK_a[e]	M^{-1} s^{-1}	s^{-1}	M^{-1}	s^{-1}	M^{-1}	M^{-1} s^{-1}	kJ mol^{-1}	J K^{-1} mol^{-1}
3-ClPy	2.81	2.33 ± 0.01	0.026 ± 0.003	91 ± 11[f]	9 ± 2	0.30 ± 0.08	3 ± 1	85.1 ± 0.6	48 ± 2
								85.8 ± 1.3[g]	40 ± 4[g]
Py	5.23	1.29 ± 0.02	0.019 ± 0.005	67 ± 18	5.5 ± 0.9	0.27 ± 0.05	1.5 ± 0.4	92 ± 2	66 ± 7
								92.2 ± 0.8[g]	65 ± 3[g]
4-Pic	5.99	1.27 ± 0.05	0.05 ± 0.02	25 ± 10	3.9 ± 0.03	0.44 ± 0.04	1.7 ± 0.02	88 ± 2	53 ± 6
								78 ± 8[h]	30 ± 27[h]
								86 ± 2[i]	49 ± 6[i]
DMAP	9.8				1.15 ± 0.02	1.88 ± 0.07	2.16 ± 0.09	88 ± 2[h]	52 ± 7[h]

[a]3-ClPy = 3-chloropyridine, Py = pyridine, 4-Pic = 4-methylpyridine, DMAP = 4-dimethylaminopyridine. [b]$K_1 = k_1/k_{-1}$ (eq 1). [c]K_2 (eq 3). [d]$k_f = k_3K_2$ = overall rate equation (eq 4). At low ligand concentrations the interchange mechanism will give a linear second-order rate behavior, i.e., $k_f = k_1$. [e]Refs 62, 63. [f]K_1 = 153 ± 17 M^{-1} determined from Abs. vs [3-chloropyridine] data (Figure 1). [g]Global fit to exponential form of Eyring equation: k_{obs} (eq 2) vs T vs [L], ignoring contribution by k_{-1}. [h]Calcd. using k_3. [i]Calcd. using k_f.

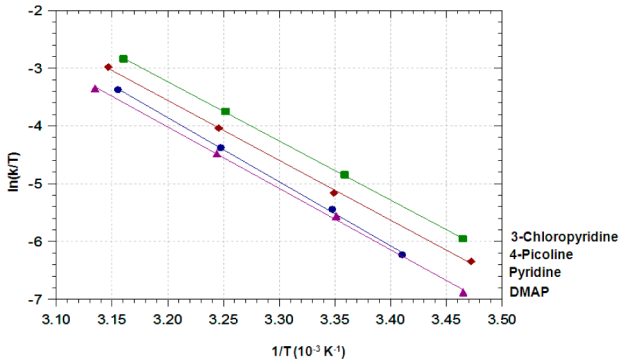

Figure 4. Eyring plots [ln(k/T) vs $1/T$] for the reaction of *fac*-[Re(Sal-*m*Tol)(CO)$_3$(HOCH$_3$)] with various pyridine type ligands in methanol.

small salicylidene (SalH) backbone. All efforts to synthesize *fac*-[Re(*L,L′*-Bid)(CO)$_3$(L)] (L = H_2O, Br^-, Py) from aqueous medium proved unsuccessful, yielding impure product mixtures as previously reported.[21] The use of methanol as a solvent proved highly successful and allows the synthesis of crystallographically pure complexes in high yield. The coordinated methanol ligand is easily substituted by other neutral entering ligands in agreement with the [2 + 1] approach.[16] This procedure creates another exciting possibility for the development of a radiopharmaceutical kit using the [2 + 1] approach with this type of ligand system.

All methanol compounds were synthesized by first subjecting [Et_4N]$_2$[Re(CO)$_3$Br$_3$] to three equivalents of $AgNO_3$, and after approximately one day of stirring at room temperature all three bromide ligands are replaced by methanol, as confirmed by mass analysis of the precipitated AgBr. Attempts to crystallize the *fac*-[Re(CO)$_3$(HOCH$_3$)$_3$]$^+$ complex have to date been unsuccessful. The formation and purity of the *fac*-[Re(Sal)(CO)$_3$(HOCH$_3$)] complexes were confirmed by IR, ^{1}H and ^{13}C NMR as well as X-ray diffraction. The Re(I) complexes yield pure crystalline products at low temperature and are stable for several months when stored under an inert atmosphere.

Spectroscopy. The complexes *fac*-[Re(*L,L′*-Bid)(CO)$_3$(L)] were characterized in situ by UV–vis and IR spectroscopy, and the data is reported in Table 1. Only one reaction was observed during the kinetic runs, and the spectra of the kinetic products agreed with that of the synthesized monosubstituted rhenium products. The IR data for reactants and some products are additionally reported which have been obtained from solid state analysis.

The complexes show typical UV–vis spectra for the low-spin d^6 metal Re(I) center under the influence of the strong ligand field affected by the *fac*-tricarbonyl orientation.[55] Typical UV–vis transitions are observed after monodentate ligand substitution has occurred. The UV–vis data (transitions and molar extinction coefficients) vary in a systematic manner for the *L,L′*-Bid ligands from **6**, **4**, **7** for the most expected electron donating ligand SalH-*p*Tol to the least SalH-*m*Tol.[56,57]

The IR data reported in Table 1 show a systematic decrease in the wave numbers for the carbonyl stretching bands from the methanol coordinated complex to the pyridine coordinated complex for **4**. However, the reverse is observed for **7**, the reason for this is currently unknown. A clear decrease in the carbonyl stretching frequency has been noted for reported *fac*-[Re(*L,L′*-Bid)(CO)$_3$(L)] complexes (L = H_2O, pyridine-type ligands, Br^-) in agreement with the ligand strength.[17,58−62] All ^{1}H NMR spectra exhibit a strong peak at approximately 8 ppm for the imine proton. An upfield shift is noted for substituted products.

X-ray Crystallography. The X-ray crystal structures for **4**, **6**, **7**, and **8** were determined and crystallographic data, selected bond distances, and bond angles are reported in Tables 2 and 3. The complex structures of **4**, **6**, **7**, and **8** are shown in Figure 5a–d respectively, with the corresponding atom numbering schemes. The bond distance from Re(I) to the monodentate ligands are indicated in Table 3 as Re-L.

The structure of **6** was difficult to obtain since the crystals lose crystallinity rapidly once removed from the mother liquid. The structure of **6** is also disordered, which underlines the flexibility of the molecule in crystallization. The *p*-tolyl substituent is disordered over two positions with a 0.57(6): 0.43(6) ratio. The aromatic ring is disordered (i.e., rotating back and forward) along the axis defined by the N1, C21A, C24A atoms with these three atoms containing a 100% occupancy, see Figure 5b. The coordinated methanol is also disordered over two positions with an occupancy ratio of 0.69(5): 0.31(5). O04B occupies a different position to O04A with a larger deviation from an ideal octahedron as manifested by the C03–Re1–O04B angle of 173.0(12)° vs. C03–Re1–O04A angle of 176(3)°.

The structures of the four complexes presented have distorted octahedral configurations around the Re(I) metal center consisting of the *N,O* bidentate ligand, three facial carbonyl ligands, and either a methanol (**4**, **6**, **7**) or a pyridine ligand (**8**). The three methanol coordinated compounds **4**, **6**, and **7** all crystallize in the monoclinic space group, *C*2/*c*, with the respective asymmetric units consisting of one parent molecular

dx.doi.org/10.1021/ic401115j | Inorg. Chem. 2013, 52, 8950−8961

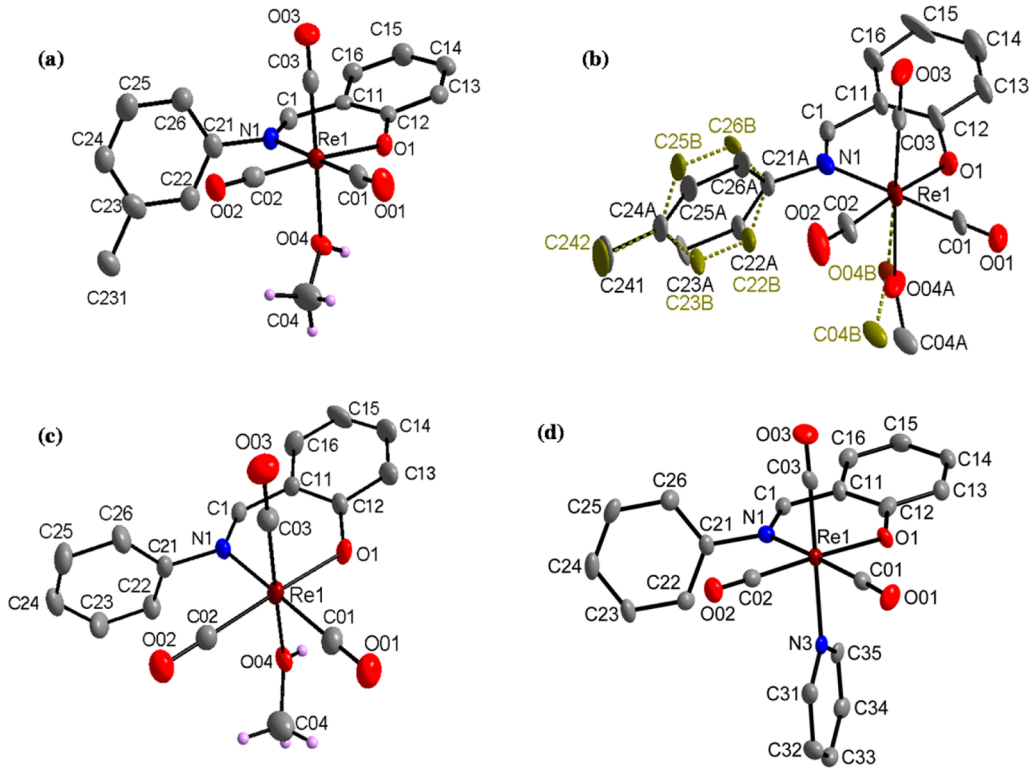

Figure 5. Molecular structures of the rhenium complexes (a) *fac*-[Re(Sal-*m*Tol)$(CO)_3(HOCH_3)$] (**4**), (b) *fac*-[Re(Sal-*p*Tol)$(CO)_3(HOCH_3)$] (**6**), (c) *fac*-[Re(Sal-Ph)$(CO)_3(HOCH_3)$] (**7**), (d) *fac*-[Re(Sal-Ph)$(CO)_3$(Py)] (**8**). Only complexes indicated, H-atoms (except for the methanol protons) are omitted for clarity.

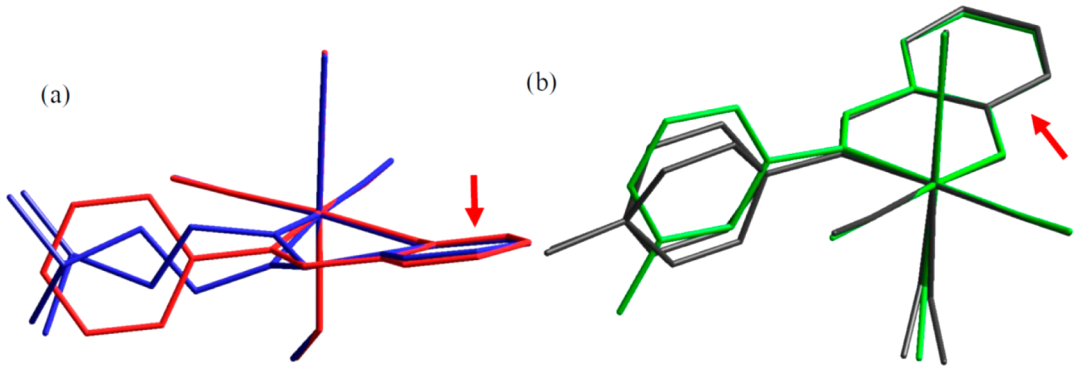

Figure 6. Graphical overlay of rhenium complexes. Overlay was not drawn through disordered substituents coordinated to the N atom of the salicylidene backbone to allow free rotation. (a) *fac*-[Re(Sal-Ph)$(CO)_3(HOCH_3)$] (**7**) (red) and *fac*-[Re(Sal-3MeBu)$(CO)_3(HOCH_3)$] (blue; wherein there was also a disorder observed; both fragments included)[21] (reproduced with permission from CSD, number 801586). (b) *fac*-[Re(Sal-*m*Tol)$(CO)_3(HOCH_3)$] (**4**) (green) and *fac*-[Re(Sal-*p*Tol)$(CO)_3(HOCH_3)$] (**6**) (black; disordered fragments included).

compound. The three compounds are iso-structural to each other as well as to the published structure *fac*-[Re(Sal-3MeBu)$(CO)_3(HOCH_3)$].[21] It is of interest to note that the orientation of the aryl substituent bonded to the imine nitrogen atom is in similar orientations in all four different molecules despite disordered atoms in two structures, that is, the *N,O*-backbone is bent toward the apical carbonyl ligand, away from the coordinated methanol, see Figure 6. The twisting of the *N,O*-backbone (defined by the plane C11, C12, C13, C14, C15, C16) relative to the coordination plane of the metal polyhedron (O1, N1, C01, C02, and Re1) varies from 15(1)°, 18.3(7)°, and 18.5(2)° for **4**, **6**, and **7**, respectively, to only 12.0(1)° for **8**.

The Re−N bond distances [(**4**) 2.157(4) Å; (**6**) 2.15(2)Å; (**7**) 2.164(6) Å; (**8**) 2.152(5) Å] and Re−O bond distances [(**4**) 2.119(3) Å; (**6**) 2.133(16)Å; (**7**) 2.121(5) Å; (**8**) 2.114(3) Å] compare well with that found for related complexes ranging from 2.152−2.199 Å for Re−N and 2.093−2.184 Å for Re−O.[17−20] The N−Re−O bite angle formed by the bidentate ligand and the Re(I) metal center [(**4**) 84.6(1)°; (**6**) 84.8(7)°; (**7**) 84.4(2)°; (**8**) 84.5(2)°] is similarly comparable to related 6-membered cyclic bidentate ligands which range from 79.1−86.2° and are approximately 10 degrees larger than for related 5-membered N−Re−O bite angles.[63]

The bond distance of rhenium to O04, the methanol oxygen [(**4**) 2.179(3) Å; (**6**) 2.17(3)−2.24(10) Å; (**7**) 2.188(5) Å], is slightly longer than that found for Re−OH_2 bonds, where the distances to the water oxygen range between 2.153−2.170 Å[17,64,65] for related Re(*N,O*-Bid) complexes. The bond distance

dx.doi.org/10.1021/ic401115j | *Inorg. Chem.* 2013, 52, 8950−8961

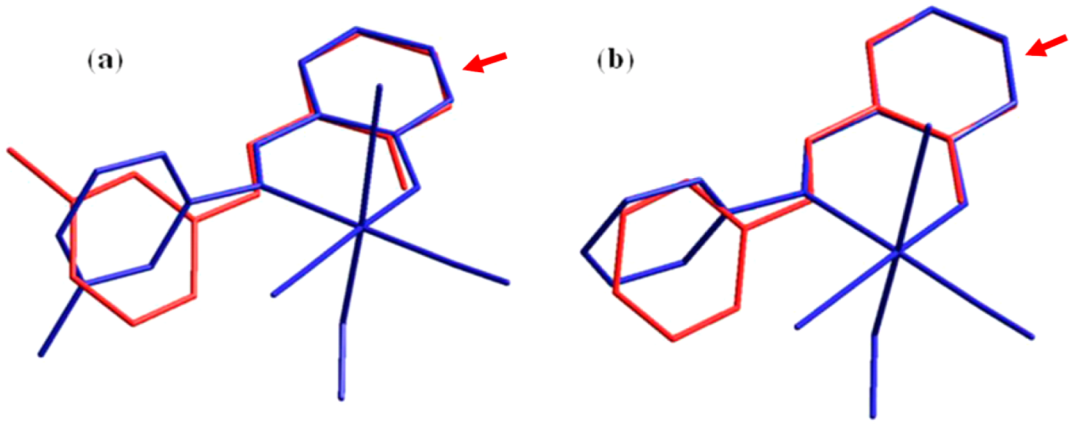

Figure 7. Graphical representation of an overlay of crystal structure (blue) and DFT optimized structure (red). (a) Crystal structure **4** (blue) and optimized free ligand **1*** (red) (RMS value = 1.391 Å). (b) Crystal structure **7** (blue) and optimized free ligand **3*** (red) (RMS value = 0.473 Å). Overlay fits exclude all hydrogen atoms.

is similar to *fac*-[Re(Flav)$(CO)_3(HOCH_3)$] (2.204(4) Å) and to a *fac*-[Tc(*N*)(*N*′)$(CO)_3(HOCH_3)]^+$ complex[66] (2.1773 Å) and compares well with other Re−O bonds.[67,68]

All the rhenium structures exhibit extensive hydrogen bonding networks with neighboring molecules (see Supporting Information) and have interactions common to all structures. π-Stacking, with an average centroid to centroid distance of 3.63 Å [3.627(3) Å, 3.752(14) Å, and 3.648(4) Å] is observed in **4**, **6**, and **7** between the salicylidene C1 aromatic backbone of neighboring molecules. Despite the abundance of aromatic rings in **8**, no π-stacking is observed.

Computational Results. An interesting aspect of noncoordinated salicylidene ligands is the different possible conformations which can be adopted in the solid state. Tautomerism between the phenol imine (O−H···N) and the keto-amine (O···H−N) forms can occur, depending on the intramolecular hydrogen bonding. Studies on thermochromic and photochromic Schiff-base compounds has resulted in the proposal that rotation around the −C═N− bond influences the specific properties, with planar molecules exhibiting thermochromism and nonplanar molecules exhibiting photochromism. The various polymorphs of 2-(phenyliminomethyl)phenol have been isolated and reported.[69,70] The conformations of the organic ligand are not the subject of discussion in this paper. However a bulky biologically active amine moiety coordinated to the imine N atoms may sterically prevent the coordination of the ligand to the Re(I) metal center. Theoretical calculations are presented here on the optimized gas-phase orientations of the free salicylidene ligands and are compared to the solid state structures of the coordinated rhenium complexes to investigate the degree of rotation around the −C═N− bond and the flexibility required to allow for metal coordination.

The noncoordinated free ligand SalH-*m*Tol (**1**) (solid state structure; see Supporting Information, Figure S1) where SalH-*m*Tol =2-(*m*-tolyliminomethyl)phenol is compared to the corresponding DFT optimized structure (**1***, Supporting Information, Figure S2; virtually identical) on the one hand; and when coordinated to the rhenium as in **4**, see Figure 7a. The same action was repeated by using SalH-Ph and superimposing the optimized structure (**3***, DFT) with that when coordinated to the rhenium, as in **7**, see Figure 7b. The good agreement between the rigid parts in the metal complexes in both *fac*-[Re(Sal-*m*Tol)$(CO)_3(HOCH_3)$] and complexes *fac*-[Re(Sal-Ph)$(CO)_3(HOCH_3)$], and the flexibility at the phenyl substituents, are obvious. The coordinated ligands experience a significant sterically induced twist and rotation of more than 40° around the C═N double bond as manifested by the corresponding changes in dihedral angle between the aromatic rings of 39.6° (**1***) and 39.6° (**3***) vs 81.9(2)° (**4**) and 88.5(3)° (**7**) when compared to the noncoordinated free ligands.

Substitution Kinetics. The substitution of methanol in *fac*-[Re(*L*,*L*′-Bid)$(CO)_3(HOCH_3)$] by a range of entering monodentate ligands was investigated under pseudo first-order conditions defined initially by the overall equilibrium as indicated in eq 1. The characterization of starting reagents and substitution products were confirmed by the chemical and spectroscopic analyses, as well as by X-ray structure determinations as described above. Different substituted pyridines (3-chloropyridine, pyridine, 4-picoline, and 4-dimethylaminopyridine) were selected as the monodentate entering ligands because of their seven orders-of-magnitude range of pK_a values (2.81, 5.23, 5.99, and 9.8) and thus significant change in electron donating abilities.[71,72] Preliminary kinetic studies were conducted using Br^- (in the form of NaBr or $[Et_4N]Br$) as entering ligand; however, no reaction was observed. From synthetic experiments, it is known that the reaction of $[Et_4N]_2[Re(CO)_3(Br)_3]$ with the SalH ligands results in methanol replacing bromide in the third position. It should therefore not be unsurprising that in an excess [Br^-], bromide ions do not readily re-enter the coordination sphere since the stability constants of the *fac*-[Re(*L*,*L*′-Bid)$(CO)_3$(**Br**)] are much lower than those of the corresponding methanol species.[17]All complexes described here have stable six-membered chelating ligand systems, and the SalH ligand remains coordinated to the Re metal center even in the presence of excess pyridine. Other preliminary studies with imidazole were conducted, however the spectral changes (despite increasing the Re complex concentration) were considered too small to yield accurate results and were not pursued further. Kinetic studies were first attempted on a UV−vis spectrophotometer, but the fast rates for most of the reactions resulted in the loss of a large part of the Abs. vs time traces. All kinetic measurements were therefore monitored on a stopped-flow spectrophotometer and were reproducible in both the Diode-Array and Photo-Multiplier mode. The k_{obs} versus [Ligand] plots, determined for the range of complexes (**4**, **6**, and **7**) and entering ligands used, produced linear plots in some cases but *nonlinear* ones in others. This obviously complicated the assignment of the intimate mechanism; therefore, fits of the rate data vs [L] were interpreted with

dx.doi.org/10.1021/ic401115j | *Inorg. Chem.* 2013, 52, 8950−8961

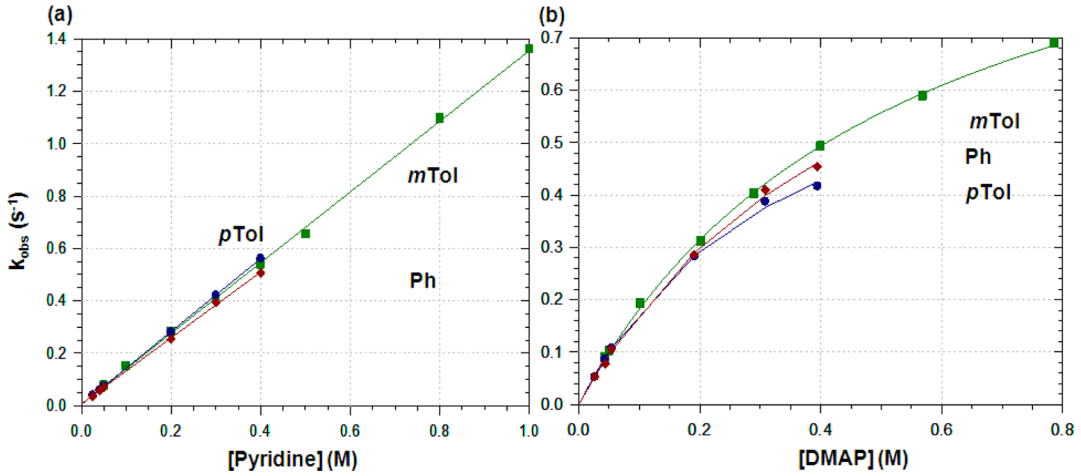

Figure 8. Plot of k_{obs} vs entering ligand for the reaction of (a) *fac*-[Re(Sal)$(CO)_3(HOCH_3)$] and pyridine at 25 °C in methanol, yielding linear plots; (b) *fac*-[Re(Sal)$(CO)_3(HOCH_3)$] and DMAP at 25 °C in methanol, yielding limiting plots.

Table 5. Rate Constants Determined for the Reaction of *fac*-[Re(Sal)$(CO)_3(HOCH_3)$] with Pyridine and DMAP at 25 °C in Methanol

complex	IR (ν_{CO}, cm^{-1})	k_1 (M^{-1} s^{-1})	K_1 (M^{-1})	k_3 (s^{-1})	K_2 (M^{-1})	$k_f = k_3K_2$ (M^{-1} s^{-1})
			Entering ligand = Pyridine			
*m*Tol	2002, 1869	1.29 ± 0.02	67 ± 18	5.5 ± 0.9	0.27 ± 0.05	1.5 ± 0.4
*p*Tol	2016, 1878	1.39 ± 0.01	372 ± 73	*31 ± 32*[a]	*0.05 ± 0.05*	*1.4 ± 2.1*
Ph	2021, 1893	1.26 ± 0.02	196 ± 117	*8 ± 5*	*0.2 ± 0.1*	*1.4 ± 1.3*
			Entering ligand = DMAP			
*m*Tol	2002, 1969			1.15 ± 0.02	1.88 ± 0.07	2.16 ± 0.09
*p*Tol	2016, 1878			0.80 ± 0.05	2.9 ± 0.3	2.3 ± 0.3
Ph	2021, 1893			1.03 ± 0.08	2.0 ± 0.2	2.1 ± 0.3

[a]Values with large ESDs (*indicated in italics*) are given for qualitative purpose only.

eqs 1 and 3, as expected for a pure Associative or an Interchange mechanism, respectively. The reverse reaction rates (k_{-3}) from eq 4 were initially determined for all reactions; however, the near zero values (approximates to zero within standard deviation) were considered insignificant and are therefore not included in the tables listed.

The methanol substitution reaction of *fac*-[Re(Sal-*m*Tol)-$(CO)_3(HOCH_3)$] with different pyridine-type entering ligands with a large difference in electron donating abilities were obtained at four different temperatures, see Figure 3. Linear plots with no obvious tendency of curvature were found for 3-chloropyridine and pyridine, the ligands with the lowest pK_a values (2.81, 5.23).[63] Data obtained for 4-picoline indicates slight curvature (pK_a = 5.99), whereas the reaction with DMAP (pK_a = 9.8) indicates distinct curvature with near saturation limits, see Figure 3c. The equilibrium constant, K_1, for the reaction of *fac*-[Re(Sal-*m*Tol)$(CO)_3(HOCH_3)$] and 3-chloropyridine was large at all four temperatures studied, indicating favorability toward the forward reaction. The large standard deviation on the k_{-1} value however increases the uncertainty of the equilibrium constant; therefore, the equilibrium constant was also determined individually from the absorbance vs ligand concentration plots (Figure 1) (K_1 = 153 ± 17 M^{-1}) and is comparable, within experimental error, with the kinetically determined value of 91 ± 11 M^{-1} as obtained for the data fits to eq 1.

The k_1, k_{-1}, and K_1 values were calculated for the reaction of *fac*-[Re(Sal-*m*Tol)$(CO)_3(HOCH_3)$] with DMAP, albeit that the data indicates the most significant curvature, using the four lowest concentrations. This resulted in rate constants with very high standard deviations. The second-order rate constant (k_1) was nevertheless compared to the forward rate constant, k_f, and a fair agreement is obtained (see Table 4). The second-order rate constant determined at 46 °C is significant when compared to k_f (k_1 = 18.3 ± 0.1 M^{-1} s^{-1}, k_{-1} = 0.015 ± 0.004 s^{-1}, K_1 = (1.22 ± 0.3) × 10^3 M^{-1}) and agrees particularly well.

All calculated second-order rate constants determined from eqs 2 and 4 for either an associative- or interchange-type mechanism, decrease in the order 3-ClPy > Py > 4-Pic > DMAP, see Figure 3c. This tendency is inversely proportional to the pK_a values of the ligands, which is contrary to what is expected for an associative type mechanism. The linear plots for 3-ClPy and Py could indicate an associative (A) or interchange associative (I_a) mechanism; however, the positive values for entropy of activation $\Delta S^{\ddagger}$ (Table 4) point to a dissociative or I_d type mechanism. A very important observation for these results, assuming an I_d mechanism, is manifested in the stepwise increase in the pre-equilibrium constant (K_2), in direct agreement with the Bronsted acid−base properties, i.e. electron density on the entering N-atom of the pyridine type ligand. This is considered good supporting evidence for an I_d mechanism. At low ligand concentrations the interchange and dissociative mechanisms will give a linear second-order rate behavior, that is, $k_f = k_1 = k_3K_2$. The forward rate constant (k_f) for an interchange mechanism is similar to the second-order rate constant (k_1) within experimental error as indicated in Table 4.

The second order rate constant (k_1) obtained for the reaction of *fac*-[Re(Sal-*m*Tol)$(CO)_3(HOCH_3)$] with pyridine (k_1= 1.29

dx.doi.org/10.1021/ic401115j | *Inorg. Chem.* 2013, 52, 8950−8961

± 0.02) M^{-1} s^{-1}) is larger than the reactions studied by Schutte et al.[17] for analogous *N,O*-bidentate ligands (*fac*-[Re(Pico)-$(CO)_3(H_2O)$] $k_1 = (1.6 \pm 0.1) \times 10^{-3}$ M^{-1} s^{-1}; *fac*-[Re(Quin)$(CO)_3(H_2O)$] $k_1 = (3.9 \pm 0.1) \times 10^{-3}$ M^{-1} s^{-1}; *fac*-[Re(2,4-PicoH)$(CO)_3(H_2O)$] $k_1 = (1.641 \pm 0.008) \times 10^{-3}$ M^{-1} s^{-1}; *fac*-[Re(2,4-QuinH)$(CO)_3(H_2O)$] $k_1 = (3.31 \pm 0.02) \times 10^{-3}$ M^{-1} s^{-1}), where Pico = 2-picolinate, Quin = 2-quinolinate, 2,4-PicoH = 2,4-pyridinedicarboxylate, 2,4-QuinH = 2,4-quinolinedicarboxylate. The Sal-type Schiff base ligands therefore activate the Re(I) metal center considerably more than the aforementioned other *N,O*-donor ligands.

Following the results obtained with *fac*-[Re(Sal-*m*Tol)-$(CO)_3(HOCH_3)$] and to investigate the ***electronic*** manipulation of the ligand backbone substituents on the rate constants and the mechanism, only two ligands (DMAP and Py) were selected to continue the kinetic study. Thus, the methanol substitution reaction of *fac*-[Re(Sal-***p*Tol**)$(CO)_3(HOCH_3)$] and *fac*-[Re(Sal-**Ph**)$(CO)_3(HOCH_3)$], wherein the steric difference of the phenyl substituents, *p*-methyl vs H was negligible (but significant electronic increase was induced) with different concentrations of 4-dimethylaminopyridine, DMAP ($pK_a = 9.8$) and pyridine, ($pK_a = 5.23$) were investigated in more detail at 25 °C. The results are illustrated in Figure 8, and the data are reported in Table 5. Linear plots were obtained for all complexes with the substitution of methanol by pyridine. Nonlinear, limiting plots were obtained for the reaction with DMAP and therefore the linear second-order rate constant k_1, could not be obtained within reasonable error. Because of the linearity of the reaction with pyridine, rate constants with large experimental errors were obtained for the interchange mechanism. The values (indicated in *italics*) are listed for completeness of the study but should be considered with caution.

Very fast reactions occurred for all the *N,O* salicylidene activated rhenium complexes. The second-order rate constants for these Schiff-base carbonyl complexes are significantly larger that those found for *N,O*-, *N,N′*-, and *O,O′*-bidentate rhenium complexes[17] with the exception of *fac*-[Re(Flav)$(CO)_3(H_2O)$] (Flav = 3-hydroxyflavonate) whose rate constant (k_1) with pyridine is of similar magnitude. The current data suggest that the prime influence toward the metal activation is from the basic Schiff-base backbone, with a much smaller contribution from the substituents thereupon.

Activation Parameters and Mechanism Assignment. The assignment of the intimate mechanism for the substitution reactions is not straightforward. However, in our opinion, the results convincingly point toward an I_d mechanism, as discussed systematically in the following paragraphs.

(i) The range of entering ligands used do not differ substantially, apart from its relative electron density as defined by the Brønsted pK_a values, that is, the donor groups are similar. One would therefore expect the intimate mechanism for all the reactions to be similar, or at the very least only point to a subtle change over, for example, $I_a \rightarrow I_d$.

(ii) Nonlinear plots were found for the reaction of DMAP with all the rhenium complexes. In particular, the reaction of *fac*-[Re(Sal-*m*Tol)$(CO)_3(HOCH_3)$] with both DMAP and 4-picoline yielded nonlinear plots. The saturation kinetics is an indication of an interchange or a dissociative mechanism.

(iii) However, the extrapolated plots of k_{obs} vs [Ligand] for the reactions with the different ligands showed saturation at *different* values, thus excluding a pure dissociative mechanism (different ligands require saturation at the *same* limiting value).

(iv) Thus, the most likely mechanism is considered to be an interchange dissociative mechanism (I_d) as further supported by the positive values determined for the entropy of activation ($\Delta S^{\ddagger}$), whereby there is an interchange of the coordinated methanol S and L within the outer-sphere complex (Re-(MeOH)···L) to form a rapid pre-equilibrium, followed by a slower, rate-determining second reaction.

A small discrepancy was in principle observed in the reaction of *fac*-[Re(Sal-*m*Tol)$(CO)_3(HOCH_3)$] with DMAP. A methyl functionality in the *meta* position is expected to introduce less electron density than the *para* position, therefore *fac*-[Re(Sal-*p*Tol)$(CO)_3(HOCH_3)$] should be more electron rich than *fac*-[Re(Sal-*m*Tol)$(CO)_3(HOCH_3)$]; however, the rate (k_3) for *fac*-[Re(Sal-*p*Tol)$(CO)_3(HOCH_3)$] is the slower of the two complexes. However, upon consideration of the overall net reaction ($k_f = k_3K_2$) the *p*Tol complex is indeed faster, albeit only just, which suggests that the electron density variation is probably too small to induce a significant observable effect. From the crystallographic data there is no significant difference in the Re−O_{04} bond distance which could explain the kinetic results (*p*Tol complex Re−O_{04} = 2.17(3) Å vs *m*Tol complex Re−O_{04} = 2.179(3) Å).

Finally, although the complexes show prominent IR stretching frequencies, there is no systematic dependence on the bidentate ligand properties. The Re−OH−CH_3 bond angle (determined from crystallographic studies) is not significantly different when comparing the aromatic complexes [*p*Tol (123.6(19)°), Ph (121.2(5)°), and *m*Tol (122.1(3)°)].

■ CONCLUSIONS

The effect of the *N,O* salicylidene bidentate ligands on the reactivity of the Re(I) metal center was illustrated by the use of *m*-tolyl, *p*-tolyl, and phenyl substituents coordinated to the imine N atom of the bidentate ligand. Few Re(I) tricarbonyl complexes containing the salicylidene bidentate ligand have been reported and none have investigated the kinetic activity effects. The ability of Schiff bases to introduce significant electron density to transition metal centers in general is widely known. The Schiff base ligand clearly introduces much more electron density to the rhenium metal center than the aqua ligands in *fac*-[Re-$(CO)_3(H_2O)_3]^+$ and thus increases the dissociative ability of the coordinated ligands (i.e., the methanol in the current study). Significant activation of the Re(I) metal center occurred yielding rapid substitution reactions, as manifested by the 3 orders of magnitude increase in reaction rate, which have previously only been reported for the *O,O′*-bidentate flavanoid-type ligand. It is clear that the *N,O*-Sal-type ligands also activate the Re(I) metal center significantly, allowing for the first time the novel opportunity to evaluate substitution reactions under limiting conditions in these tricarbonyl complexes, that is, by exhibiting nonlinear reaction rate profiles, indicating an interchange activation for the process.

■ ASSOCIATED CONTENT

Ⓢ Supporting Information

All the kinetic data, including k_{obs} values and temperature studies for the complexes of **4**, **6**, and **7**. This material is available free of charge via the Internet at http://pubs.acs.org. Crystallographic data for the structures **4**, **6**, **7**, and **8** are available free of charge from the Cambridge Crystallographic Data Centre via www.ccdc.cam.ac.uk/data_request/cif as CCDC 946633−946636.

dx.doi.org/10.1021/ic401115j | *Inorg. Chem.* 2013, 52, 8950−8961

AUTHOR INFORMATION

Corresponding Author

*E-mail: roodta@ufs.ac.za. Phone: +27 51 4012547. Fax +2751 4446384.

Notes

The authors declare no competing financial interest.

ACKNOWLEDGMENTS

Financial assistance from the University of the Free State is gratefully acknowledged. Prof. Ola F. Wendt from the University of Lund, Sweden, is thanked for the use of their Oxford X-ray diffractometer. We thank SASOL, the South African National Research Foundation (SA-NRF/THRIP), the University of the Free State Strategic Academic Cluster Initiative (Advanced Biomolecular Research and the Materials and Nanosciences Clusters), and the Swedish International Development Cooperation Agency (SIDA) for financial support of this project.

REFERENCES

(1) Liu, S.; Edwards, D. S. *Chem. Rev.* **1999**, *99*, 2235−2268.
(2) Liu, S. *Chem. Soc. Rev.* **2004**, *33*, 445−461.
(3) Alberto, R.; Schibli, R.; Egli, A.; Schubiger, A. P.; Herrmann, W. A.; Artus, G.; Abram, U.; Kaden, T. A. *J. Organomet. Chem.* **1995**, *493*, 119−127.
(4) Egli, A.; Alberto, R.; Tannahill, L.; Schibli, R.; Abram, U.; Shaffland, A.; Waibel, R.; Tourwé, D.; Jeannin, L.; Iterbeke, K.; Schubiger, A. P. *J. Nucl. Med.* **1999**, *40*, 1913−1917.
(5) Alberto, R.; Schibli, R.; Schubiger, A. P.; Abram, U.; Pietzsch, H. J.; Johannsen, B. *J. Am. Chem. Soc.* **1999**, *121*, 6076−6077.
(6) Spradau, T. W.; Edwards, W. B.; Anderson, C. J.; Welch, M. J.; Katzenellenbogen, J. A. *Nucl. Med. Biol.* **1999**, *26*, 1−7.
(7) Xavier, C.; Jae-Kyoung, P.; Santos, I.; Alberto, R. *J. Organomet. Chem.* **2007**, *692*, 1332−1339.
(8) Schibli, R.; Schubiger, P. A. *Eur. J. Nucl. Med.* **2002**, *29*, 1529−1542.
(9) Maria, L.; Cunha, S.; Videira, M.; Gano, L.; Paulo, A.; Santos, I. C.; Santos, I. *Dalton Trans.* **2007**, 3010−3019.
(10) Wirth, S.; Wallek, A. U.; Zernickel, A.; Feil, F.; Sztiller-Sikorska, M.; Lesiak-Mieczkowska, K.; Bräuchle, C.; Lorenz, I. P.; Czyz, M. *J. Inorg. Biochem.* **2010**, *104*, 774−789.
(11) Alberto, R.; Schibli, R.; Waibel, R.; Abram, U.; Schubiger, A. P. *Coord. Chem. Rev.* **1999**, *190−192*, 901−919.
(12) Salignac, B.; Grundler, P. V.; Cayemittes, S.; Frey, U.; Scopelliti, R.; Merbach, A. E. *Inorg. Chem.* **2003**, *42*, 3516−3526.
(13) Grundler, P. V.; Salignac, B.; Cayemittes, S.; Alberto, R.; Merbach, A. E. *Inorg. Chem.* **2004**, *43*, 865−873.
(14) Grundler, P. V.; Helm, L.; Alberto, R.; Merbach, A. E. *Inorg. Chem.* **2006**, *45*, 10378−10390.
(15) Helm, L. *Coord. Chem. Rev.* **2008**, *252*, 2346−2361.
(16) Mundwiler, S.; Kündig, M.; Ortner, K.; Alberto, R. *Dalton Trans.* **2004**, 1320−1328.
(17) Schutte, M.; Kemp, G.; Visser, H. G.; Roodt, A. *Inorg. Chem.* **2011**, *50*, 12486−12498.
(18) Schutte, M.; Roodt, A.; Visser, H. G. *Inorg. Chem.* **2012**, *51*, 11996−12006.
(19) Faller, J. W.; Mason, G.; Par, J. *J. Organomet. Chem.* **2001**, *626*, 181−185.
(20) Czerwieniec, R.; Kapturkiewicz, A.; Anulewicz-Ostrowska, R.; Nowacki, J. *J. Chem. Soc., Dalton Trans.* **2002**, 3434−3441.
(21) Li, Z. K.; Ki, Y.; Lei, L.; Che, C. M.; Zhou, X. G. *Inorg. Chem. Commun.* **2005**, *8*, 307−309.
(22) Brink, A.; Visser, H. G.; Roodt, A. *J. Coord. Chem.* **2011**, *64*, 122−133.
(23) Roodt, A.; Leipoldt, J. G.; Helm, L.; Abou-Hamdan, A.; Merbach, A. E. *Inorg. Chem.* **1995**, *34*, 560−568.
(24) Abou-Hamdan, A.; Roodt, A.; Merbach, A. E. *Inorg. Chem.* **1998**, *37*, 1278−1288.
(25) Roodt, A.; Abou-Hamdan, A.; Engelbrecht, H. P.; Merbach, A. E. *Adv. Inorg. Chem.* **1999**, *40*, 59−126.
(26) Roodt, A.; Leipoldt, J. G.; Helm, L.; Merbach, A. E. *Inorg. Chem.* **1994**, *33*, 140−147.
(27) Alberto, R.; Egli, A.; Abram, U.; Hegetschweiler, K.; Gramlich, V.; Schubiger, P. A. *J. Chem. Soc., Dalton Trans.* **1994**, 2815−2820.
(28) Gibson, D. H.; Sleadd, B. A.; Yin, X. *Organometallics* **1998**, *17*, 2689−2691.
(29) Czerwieniec, R.; Kapturkiewicz, A.; Anulewicz-Ostrowska, R.; Nowacki, J. *J. Chem. Soc., Dalton Trans.* **2001**, 2756−2761.
(30) Alberto, R.; Egli, A.; Abram, U.; Hegetschweiler, K.; Gramlich, V.; Schubiger, P. A. *J. Chem. Soc., Dalton Trans.* **1994**, 2815−2820.
(31) Alberto, R.; Schibli, R.; Schubiger, P. A.; Abram, U.; Kaden, T. A. *Polyhedron* **1996**, *15*, 1079−1089.
(32) Brink, A.; Roodt, A.; Visser, H. G. *Acta Crystallogr.* **2009**, *E65*, o3175−o3176.
(33) Arod, F.; Gardon, M.; Pattison, P.; Chapuis, G. *Acta Crystallogr.* **2005**, *C61*, o317−o320.
(34) *APEX2* (Version 1.0−27); Bruker AXS Inc.: Madison, WI, 2005.
(35) *COSMO* (Version 1.48); Bruker AXS Inc.: Madison, WI, 2003.
(36) *SAINT-Plus (including XPREP)* (Version 7.12); Bruker AXS Inc.: Madison, WI, 2004.
(37) *SADABS* (Version 2004/1); Bruker AXS Inc.: Madison, WI, 1998.
(38) *Crysalis CCD*; Oxford Diffraction Ltd.: Abingdon, Oxfordshire, U.K., 2005.
(39) *Crysalis RED*; Oxford Diffraction Ltd.: Abingdon, Oxfordshire, U.K., 2005.
(40) Altomare, A.; Burla, M. C.; Camalli, M.; Cascarano, G. L.; Giacovazzo, C.; Guagliardi, A.; Moliterni, A. G. G.; Polidori, G.; Spagna, R. *J. Appl. Crystallogr.* **1999**, *32*, 115−119.
(41) Farrugia, L. J. *J. Appl. Crystallogr.* **1999**, *32*, 837−838.
(42) Sheldrick, G. M. *SHELXL97, Program for Solving Crystal Structures*; University of Göttingen: Göttingen, Germany, 1997.
(43) Brandenburg, K.; Putz, H. *DIAMOND*, Release 3.0c; Crystal Impact GbR: Bonn, Germany, 2005.
(44) *Hyperchem, Windows Molecular Modeling System*, Release 7.52; Hypercube, Inc.: Gainesville, FL, 2002.
(45) Van der Westhuizen, H. J.; Meijboom, R.; Roodt, A.; Schutte, M. *Inorg. Chem.* **2010**, *49*, 9599−9608.
(46) Roodt, A.; Leipoldt, J. G.; Deutsch, E. A.; Sullivan, J. C. *Inorg. Chem.* **1992**, *31*, 1080−1085.
(47) *Micromath Scientist for Windows*, Version 2.01; MicroMath Inc.: Saint Louis, MI, 1986−1995.
(48) Swaddle, T. W. *Adv. Inorg. Bioinorg. Mech.* **1983**, *2*, 95−138.
(49) Wilkins, R. G. *Kinetics and Mechanism of Reactions of Transition Metal Complexes*, 2nd ed.; VCH Publishers, Inc.: New York, 2002.
(50) Muller, A.; Otto, S.; Roodt, A. *Dalton Trans.* **2008**, 650−657.
(51) Frisch, M. J.; Trucks, G. W.; Schlegel, H. B.; Scuseria, G. E.; Robb, M. A.; Cheeseman, J. R.; Montgomery Jr., J. A.; Vreven, T.; Kudin, K. N.; Burant, J. C.; Millam, J. M.; Iyengar, S. S.; Tomasi, J.; Barone, V.; Mennucci, B.; Cossi, M.; Scalmani, G.; Rega, N.; Petersson, G. A.; Nakatsuji, H.; Hada, M.; Ehara, M.; Toyota, K.; Fukuda, R.; Hasegawa, J.; Ishida, M.; Nakajima, T.; Honda, Y.; Kitao, O.; Nakai, H.; Klene, M.; Li, X.; Knox, J. E.; Hratchian, H. P.; Cross, J. B.; Bakken, V.; Adamo, C.; Jaramillo, J.; Gomperts, R.; Stratmann, R. E.; Yazyev, O.; Austin, A. J.; Cammi, R.; Pomelli, C.; Ochterski, J. W.; Ayala, P. Y.; Morokuma, K.; Voth, G. A.; Salvador, P.; Dannenberg, J. J.; Zakrzewski, V. G.; Dapprich, S.; Daniels, A. D.; Strain, M. C.; Farkas, O.; Malick, D. K.; Rabuck, A. D.; Raghavachari, F.; Foresman, J. B.; Ortiz, J. V.; Cui, Q.; Baboul, A. G.; Clifford, S.; Cioslowski, J.; Stefanov, B. B.; Liu, G.; Liashenko, A.; Piskorz, P.; Komaromi, I.; Martin, R. L.; Fox, D. J.; Keith, T.; Al-Laham, M. A.; Peng, C. Y.; Nanayakkara, A.; Challacombe, M.; Gill, P. M. W.; Johnson, B.; Chen, W.; Wong, M. W.; Gonzalez, C.; Pople, J. A. *GAUSSIAN-03*, Revision C.01; Gaussian, Inc.: Wallingford, CT, 2004.
(52) Becke, A. D. *J. Chem. Phys.* **2003**, *98*, 5648−5652.
(53) Hariharan, P. C.; Pople, J. A. *Theoret. Chim. Acta* **1973**, *28*, 213−222.
(54) Francl, M. M.; Petro, W. J.; Hehre, W. J.; Binkley, J. S.; Gordon, M. S.; De Free, D. J.; Pople, J. A. *J. Chem. Phys.* **1982**, *77*, 3654−3665.

(55) Cotton, F. A.; Wilkinson, G.; Gaus, P. L. *Basic Inorganic Chemistry*, 3rd ed.; John Wiley & Sons Inc.: New York, 1995.
(56) Clayden, J.; Greeves, N.; Warren, S.; Wothers, P. *Organic Chemistry*; Oxford University Press: New York, 2001.
(57) Corwin, H.; Leo, A.; Taft, R. W. *Chem. Rev.* **1991**, *91*, 165−195.
(58) Steyn, G. J. J.; Roodt, A.; Leipoldt, J. G. *Inorg. Chem.* **1992**, *31*, 3477−3481.
(59) Otto, S.; Roodt, A. *Inorg. Chim. Acta* **2004**, 1−10.
(60) Brink, A.; Roodt, A.; Steyl, G.; Visser, H. G. *Dalton Trans.* **2010**, *39*, 5572−5578.
(61) Roodt, A.; Otto, S.; Steyl, G. *Coord. Chem. Rev.* **2003**, *245*, 125−142.
(62) Hevia, E.; Pérez, J.; Riera, V.; Miguel, D. *Organometallics.* **2002**, *21*, 5312−5319.
(63) Roodt, A.; Visser, H. G.; Brink, A. *Crystallogr. Rev.* **2011**, *17*, 241−280.
(64) Schutte, M.; Visser, H. G. *Acta Crystallogr.* **2008**, *E64*, m1226−m1227.
(65) Schutte, M.; Visser, H. G.; Roodt, A. *Acta Crystallogr.* **2008**, *E64*, m1610−m1611.
(66) Zobi, F.; Spingler, B.; Fox, T.; Alberto, R. *Inorg. Chem.* **2003**, *42*, 2818−2820.
(67) Purcell, W.; Roodt, A.; Basson, S. S.; Leipoldt, J. G. *Transition Met. Chem.* **1990**, *15*, 239−241.
(68) Purcell, W.; Roodt, A.; Basson, S. S.; Leipoldt, J. G. *Transition Met. Chem.* **1989**, *14*, 5−6.
(69) Arod, F.; Gardon, M.; Pattison, P.; Chapuis, G. *Acta Crystallogr.* **2005**, *C61*, o317−o320.
(70) Arod, F.; Pattison, P.; Schenk, K. J.; Chapuis, G. *Cryst. Growth Des.* **2007**, *7*, 1679−1685.
(71) Perrin, D. D. *Dissociation Constants of Organic Bases in Aqueous Solution*; Butterworths: London, U.K., 1965; Supplement, 1972.
(72) Lide, D. R., Ed.; *CRC, Handbook of Chemistry and Physics*, 88th ed. (CD-ROM, Version 2008); CRC Press/Taylor and Francis: Boca Raton, FL, 2008.